Research Article

Joint analysis of IVD herniation and degeneration by rat caudal needle puncture model†

Carla Cunha[1,2*], Sofia Lamas[1,3], Raquel M Gonçalves[1,2], Mário A Barbosa[1,2,4]

[1] i3S – Instituto de Investigação e Inovação em Saúde, Universidade do Porto, Portugal
[2] INEB – Instituto de Engenharia Biomédica, Rua do Campo Alegre 823, 4150-180 Porto, Portugal.
[3] IBMC – Instituto de Biologia Molecular e Celular, Rua do Campo Alegre 823, 4150-180 Porto, Portugal.
[4] ICBAS – Instituto de Ciências Biomédicas Abel Salazar, Universidade do Porto, Rua Jorge Viterbo Ferreira 228, 4050-313 Porto, Portugal.

[*] Corresponding author
Email: carla.cunha@ineb.up.pt

Running title: IVD hernation and degeneration model

Author contributions statement: Carla Cunha performed the research, analysed the data and wrote the paper; Sofia Lamas participated in the in vivo research and analysed data; Raquel M Gonçalves critically revised the paper; Mário A Barbosa supervised the research study and writing of the paper. All authors have read and approved the final submitted manuscript.

†This article has been accepted for publication and undergone full peer review but has not been through the copyediting, typesetting, pagination and proofreading process, which may lead to differences between this version and the Version of Record. Please cite this article as doi: [10.1002/jor.23114]

Additional Supporting Information may be found in the online version of this article.

Received 13 July 2015; Revised 19 November 2015; Accepted 25 November 2015
Journal of Orthopaedic Research

DOI 10.1002/jor.23114

Abstract

Intervertebral disc (IVD) degeneration is responsible for various spine pathologies and present clinical treatments are insufficient. Concurrently, the mechanisms behind IVD degeneration are still not completely understood, so as to allow development of efficient tissue engineering approaches.

A model of rat IVD degeneration directly coupled to herniation is here proposed in a pilot study. Disc injury is induced by needle puncture, using two different needles gauges: a low caliber 25-G needle and a high caliber 21-G needle. Histological, biochemical and radiographic degeneration was evaluated at 2 and 6 weeks post-injury.

We show that the larger caliber needle results in a more extended histological and radiographic degeneration within the IVD, compared to the smaller one. TUNEL quantification indicates also increased cell death in the 21-G group. Analyses of collagen type I (Picrosirius red staining), collagen type II (immunofluorescence) and GAG content (Blyscan assay) indicate that degeneration features spontaneously recover from 2 to 6 weeks, for both needle types. Moreover, we show the occurrence of hernia proportional to the needle gauge. The number of CD68+ macrophages present, as well as cell apoptosis within the herniated tissue are both proportional to hernia volume. Moreover, hernias formed after lesion tend to spontaneously diminish in volume after 6 weeks. Finally, MMP3 is increased in the hernia in the 21-G group at 2 weeks. This model, by uniquely combining IVD degeneration and IVD herniation in the same animal, may help to understand mechanisms behind IVD pathophysiology, such as hernia formation and spontaneous regression.

Keywords: Intervertebral disc; histology; X-rays; coccygeal; collagen

Introduction

Intervertebral discs (IVD) are fibrocartilaginous cushions functioning as essential load-absorbers between vertebrae, while allowing mobility of the spine. Disorders related to IVD degeneration are widespread causes of morbidity and include neck and low back pain, which affects about 80% of people at some point in their lives [1]. Present treatment options consist of either a conservative approach using anti-inflammatory medication, rest and physical therapy or aggressive surgical interventions: spinal fusion, dynamic stabilization and disc arthroplasty; all are expensive and have relevant disadvantages. Different biomedical engineering techniques have been proposed and potential strategies include protein injection, gene transfer and cell therapy [reviewed in 2]. The majority of these techniques are pre-clinical-based, which need to rely on animal models that successfully reproduce the features of IVD degeneration in the human and possibly help in elucidating the initial causes of degeneration.

IVD structure and degeneration

The IVD is part of a complex biomechanical system composed of the cartilaginous endplates, the annulus fibrosus (AF) and the nucleus pulposus (NP). The NP is located at the center of the disc and is composed of an amorphous matrix of highly hydrated proteoglycans embedded in a loose network of collagen type II. The AF is composed of an outer region with highly organized, directionally oriented collagenous type I lamellae; and a larger inner AF, more fibrocartilaginous, containing less collagen and lacking the lamellar architecture of the outer AF and containing a higher proportion of proteoglycan aggregates. The transition zone between NP and AF consists of a distinct, thin acellular fibrous layer [reviewed in 2].

During tissue degeneration, the IVD undergoes a series of cellular, biomechanical and molecular changes that result in cell loss, alterations in the extracellular matrix composition and structure, whole tissue loss of function and mechanical failure of the whole disc [reviewed in 3,4].

In vivo *animal models of IVD degeneration*

Animal models have an important role in elucidating the mechanisms behind human disc degeneration, especially at an early stage, as the symptomatic clinical condition appears after the IVD has reached almost an endpoint of the pathological process. While not completely reproducing the clinical situation, animal studies may provide useful information for human subjects at earlier stages of the degenerative process. Numerous IVD degeneration models have been proposed in different animals, all dealing with a compromise between fully reproducing the complex features of human disc degeneration and questions such as simplicity, low cost, efficiency and reproducibility in the animal [reviewed in 5]. While many of them address a tissue engineering treatment strategy, we will not focus here on regeneration strategies. The scope of this work is to focus on the degeneration model alone and its clinically relevant pathological aspects.

Rat degeneration models

In the rat, different models of IVD degeneration have been developed:

1. compression: this method has been applied in the lumbar IVD using a custom-designed loading device that applied shear force for 1 or 2 weeks, which results in degenerative changes such as NP cavity loss and border disruption, observed from the histology sections [6]. Mechanical interventions to the spine are reported as resulting in morphological changes in the disc similar to those from degenerative disc disease in humans.

2. spondylosis: a cervical spondylosis model has been developed by excising the paraspinal musculature and posterior cervical spinal ligaments, causing instability of both static and dynamic cervical stabilizers, this resulting in consequent IVD degeneration characterized by increased local inflammation and apoptosis, such as that seen clinically [7]. Later, this method was adapted to the lumbar IVD by removing the sacrospinal muscles, spinous processes, supraspinous ligaments, interspinous ligaments, posterolateral 1/2 of bilateral zygapophysial joints of the L4–L6 lumbar spine through a dorsal medial approach. This method resulted in lumbar spine malalignment, disc space narrowing, and endplate calcification [8].

3. chemonucleolysis: this method is induced by injection of chondroitinase into the NP for enzymatic digestion and consequent degeneration. It has been used both at the lumbar IVDs [9] and at the caudal IVDs [10]. Both studies show reduction in disc height and proteoglycan content, as well as increased stiffness of the disc.

4. NP needle aspiration: this method relies on the aspiration of defined volumes of nucleus pulposus material for induction of IVD degeneration. It has been used in the lumbar IVD [11].

Rat disc needle puncture

This is the fifth method from our list and includes two main approaches. Method 1 - Rat lumbar disc puncture: the method to access ventrally the lumbar vertebral body has been proposed by Rousseau et al., 2004, which developed a surgical transperitoneal approach that permits the exposure of four lumbar vertebral bodies [12]. Recently, this method has been used to cause IVD degeneration by needle puncture using a microsurgical drill equivalent to a 25-G needle introduced to a depth of 2 mm and demonstrating proteoglycan loss and disc narrowing [13]. Others have used slightly different techniques, such as different needle size, depth of needle penetration [14,15].

Given the complicated surgery involved, with inherent variability in the methodology, a different approach has been proposed. Method 2 - Rat caudal disc puncture: this method has been developed by Han et al., 2008, followed by Zhang et al., 2009, after an initial report by Crevensten et al., 2004 describing the identification of the target disc by X-rays, insertion of a 29-G needle into the NP using custom fixturing and fluoroscopic guidance for injection of 15% hyaluronan gel containing MSCs [16]. Han et al., 2008 used a 20-G needle with either full penetration or half penetration to the coccygeal disc 7 and 8. Penetrative puncture resulted in a faster decrease in disc height, lower glycosaminoglycan content, and higher grades of histological degeneration. The water and hydroxyproline content of the discs did not change appreciably [17]. Zhang et al., 2009 used the same method with some alterations: caudal level 5/6 and 7/8 IVDs were punctured laterally with 18-G or 21-G needles to a depth of 5 mm from the subcutaneous surface with the aid of fluoroscopy and in both cases IVDs showed signs of degeneration in terms of MRI and histological

measurements [8]. More recently, this technique has been further optimized or simply used as originally reported. Keorochana et al., 2010 studied the effect of different needle gauges (18-G, 20-G, and 22-G) in rat caudal discs and examined the induced degenerative changes by plain radiography, MRI and histology. Proteoglycan content was assessed by alcian blue staining and immunohistochemistry for aggrecan, collagen II, and Sox-9 was performed. Results indicated larger needle gauges, especially 18-G, produced more deterioration of the disc when compared with smaller sizes, particularly with time [18].

In this study we have explored a rat model of IVD needle puncture by using 25-G and 21-G needles and characterizing along time the degenerative traits within the disc and, moreover, analysing herniation in the lesioned discs.

Materials and Methods

Animal experimentation

Male Wistar Han (Crl:WI/Han) rats at 10 weeks of age were anaesthetized by isofluorane inhalation and placed in prone position, the tail skin disinfected with ethanol and a percutaneous needle puncture performed dorsally into three consecutive coccygeal IVDs: Co5/6, Co6/7 and Co7/8, with the help of radiography for disc identification.

An incision was made at a depth of penetration of 5 mm, by use of a home-made needle cap device (Figure 1), followed by 360° rotation of the needle, hold of 30 sec, second 360° rotation of the needle, hold of 30 sec and withdrawal.

Animals were kept in a 12-hour light/dark cycle, with food and water *ad libitum* and were monitored daily for the duration of the experiments, 2 weeks or 6 weeks, with no signs of distress or pain. Gauge needles of 25-G and 21-G were used and 3 animals per group were analysed. Control group refers to littermate healthy unlesioned rats.

All animal experimentation was carried out at the IBMC.INEB animal house facility and has been approved by the IBMC.INEB Animal Ethics Committee and by Direcção Geral de Alimentação e Veterinária through licence nº 3773/2015-02-09 and conducted in accordance with the European Legislation on Animal Experimentation through Directive 2010/63/UE.

Identification of the target discs

By dorsal palpation and lateral X-ray imaging, the first coccygeal vertebra (Co1) is identified. This is the vertebra with the most prominent spinous process in this region. It is at the level of the sacroiliac joint and it is flexible with respect to the more anterior sacral vertebral body. The first coccygeal disc (Co1/2) is located between Co1 and Co2. The subsequent discs are counted by palpation and X-ray imaging, so that the target disc Co5/6 can be found (Figure 1a).

Calculation of disc height index

The animals were anesthetized and placed in prone position with their tails laid straight on the platform. Radiographs for the IVD of interest were acquired by the Owandy-RX radiology system equipped with the Opteo digital sensor (Owandy radiology), with a radiation exposure of 0.06 S/mGy and a collimator-to-tissue fixed distance of 6 cm for all animals. QuickVision software was used for processing of digital radiographies. As described before [17,19], the disc height index (DHI) was calculated from the digital radiographs by use of the ImageJ software, as the mean of the 3 measurements from midline to the boundary of the central 50% of disc width, divided by the mean of the 2 adjacent vertebral body heights (DHI=2x(D+E+F)/(A+B+C+G+H+I); Figure 2a). The %DHI was calculated by the difference in disc height index between post-puncture and pre-puncture, for each disc (%DHI=post-punctured DHI/pre-punctured DHI*100).

Tissue collection and Histological analysis

All animals were sacrificed by CO_2 inhalation and target IVDs dissected and collected for analysis. For GAG quantification, only the NP from the central part of the disc was collected. For histological analysis, IVD and adjacent vertebrae were kept *en bloc* and the whole section was fixed in 10% neutral buffered formalin (VWR) for 48 hours at room temperature. Tissue was then

decalcified in EDTA-glycerol solution and processed for paraffin embedding through ethanol series and clearing in xylene. Consecutive transversal 5 µm sections of the IVD were collected via a microtome (Leica). Tissue sections were dewaxed in xylene solution and rehydrated through a graded series of ethanol. Hematoxylin&eosin staining, as well as Masson's trichrome staining, was performed comprising the whole length of each IVD. Tissue was dehydrated in a graded series of ethanols, slides mounted with DPX (VWR) and analysed in an upright optical microscope (Olympus). For the determination of % area of proteoglycans and collagen, a custom ImageJ macro based on a color deconvolution technique was used to separate the color channels from Safranin-O and Masson's Trichrome stainings, respectively [20].

Histological grading scale

Tissue sections were stained for Safranin O & Fast Green and analysed by an upright optical microscope (Olympus). All slides were evaluated for 5 categories of IVD degenerative alterations: Cellularity of the AF, Morphology of the AF, Border between the AF and NP, Cellularity of the NP and Morphology of the NP, each classified with a score between 1 (normal disc) and 5 (highly degenerated disc). This grading score was made according to the criteria defined previously [17], that considers cellular types present and their cytomorphology and the appearance of the extracellular matrix. The overall sum of each score per category was determined for each animal and results presented as mean score per group.

Determination of hernia volume

Tissue sections were stained for Safranin O & Fast Green and images of the hernia collected by an upright optical microscope (Olympus), throughout the IVD at precise intervals. For each section, delimitation of the hernia was made by the freehand selection tool using the ImageJ software. After image scale calibration, the area of the selection in mm^2 was determined.

Hernia volume for each animal was determined from the sum of the areas of each individual section throughout the IVD, as follows: V= sum of areas * 0.005 mm (sections thickness) * 10 (number of

slide series from which the sections analysed were collected). Results are presented as mean hernia volume per group.

Collagen type II immunofluorescence

One tissue section per animal containing the central portion of the IVD was processed for immunofluorescence against Collagen type II. Antigen retrieval was performed with Proteinase K (Sigma) treatment, by incubating slides in 20 µg/ml proteinase K solution at 37°C for 15 minutes. Blocking was performed with Background block (Cell Marque) and tissue permeabilization with 0.1% (v/v) Triton X-100. Sections were incubated with the primary antibody anti-Collagen II-II6B3 (Developmental Studies Hybridoma Bank) diluted 1:20 overnight at 4°C. Primary antibody was probed with the secondary antibody Alexa Fluor\ 488 goat anti-mouse diluted 1:250 (Life Technologies) for 1 hour at room temperature. Cell nuclei counterstaining was performed by mounting slides with Fluorshield containing DAPI (Sigma). Three optical sections per animal were examined in a Zeiss Axiovert200 inverted fluorescence microscope (Zeiss). Each slide was assigned a score for the overall staining, where +=weak, ++=moderate and +++=strong.

PicroSirius red staining

A solution of Picrosirius red was prepared by diluting 3g of Sirius red (Sigma) into 500 ml of saturated aqueous solution of picric acid (Sigma). Tissue sections were dewaxed in xylene solution and rehydrated through a graded series of ethanol. Sections were then incubated in Weigert's Iron Hematoxylin for 8 minutes and washed in tap water. Sections were incubated in Picrosirius red solution for 1 hour and then washed in two changes of Acetic Acid 1%. After air-drying the slides, tissue was dehydrated and slides mounted with DPX (VWR) and analysed in a Zeiss Axiovert200 inverted microscope (Zeiss), under polarized light. Three optical sections per slide were assigned a score for the overall staining, where +=weak, ++=moderate and +++=strong.

CD68, MMP3 and MMP14 immunohistochemistry

One tissue section per animal containing the central portion of hernia site was processed for each immunohistochemistry labelling. Antigen retrieval was performed in a pressure cooker in 10

mmol/L sodium citrate buffer, pH 6.0, for 3 minutes. The Novolink™ Max-Polymer detection system (Novocastra) was used, according to the manufacturer′s instructions. Briefly, endogenous peroxidase activity was blocked with Peroxidase Block for 5 min, followed by Protein Block for 5 min. Sections were then incubated overnight at 4°C with the primary antibodies anti-CD68 clone ED1 (AbD Serotec) diluted 1:100, anti-MMP3 and anti-MMP14 (Abcam) diluted 1:100. A Post Primary solution was incubated for 30 min (only for CD68), followed by Novolink™ Polymer incubation for 30 min. Color was developed with DAB working solution and sections were then counterstained with haematoxylin, dehydrated, and mounted. Sections were examined in an upright optical microscope (Olympus). Quantification of immunoreactivity was made by counting the total number of positive cells within the hernia site and calculating the mean number for each group.

TUNEL assay

TUNEL assay was performed by use of the DeadEnd™ Fluorometric TUNEL System (Promega), according to manufacturer's instructions. Briefly, paraffin embedded tissue was dewaxed, rehydrated and permeabilized by Proteinase K (20 μg/ml) digestion for 8 minutes at room temperature. Tissue was incubated for 1 hour at 37°C with recombinant Terminal Deoxynucleotidyl Transferase and fluorescein-12-dUTP and reaction stopped by incubating slides in 2x SSC for 15 minutes. Cell nuclei counterstaining was performed by mounting slides with Fluorshield with DAPI (Sigma). Three optical sections per animal were examined in a Zeiss Axiovert200 inverted fluorescence microscope (Zeiss). The proportion of cells positive for TUNEL staining was determined for the NP and AF, by counting total number of positive cells per optical section as well as the total number of cells in the section by DAPI staining. The number of positive cells within the hernia site was determined by counting the total number of positive cells per hernia section.

Glycosaminoglycan (GAG) quantification

NPs were collected fresh using a fine spatula and their wet weight was determined immediately before snap freezing at -80ºC. The tissue was digested with papain (Sigma) at 65ºC overnight. The next day, the Blyscan sulfated proteoglycan assay (Biocolor) was used as a quantitative dye-binding

method for the analysis of sulfated proteoglycans and glycosaminoglycans and performed according to manufacturer's instructions. Briefly, 100 µl of digested sample was incubated with the Blyscan dye reagent. After releasing the dye into solution from the sGAG-dye complex, absorbance values were determined at 656 nm and plotted in a graph against a calibration curve, from which the GAG values for each sample were determined. GAG content in each sample was normalized by sample wet weight.

Statistical analysis

All results were expressed as MEAN±SD plotted on graph and statistical analysis was performed using GraphPad Prism software (version 5.0), with statistical significance set at $p \leq 0.05$. For all data, analysis of differences between samples was made by Kruskal-Wallis test, followed by Dunn's multiple comparison test between groups.

Results

In this study we have characterized the histological and biochemical features behind disc degeneration in an *in vivo* rat model of intervertebral disc needle puncture injury. Two different needles gauges were used: a low caliber 25-G needle and a high caliber 21-G needle (Figure 1). IVD degeneration was evaluated for both groups at 2 and 6 weeks post-injury. A total of 14 animals have been used, with n=3 per group.

Determination of disc height index by radiography

For all animals, IVD X-rays were collected immediately before lesion and at the end of the experimental time. Disc height index (DHI) was calculated by disc height normalized to the height of adjacent vertebra, as DHI=2x(D+E+F)/(A+B+C+G+H+I) (Figure 2a).

Changes in DHI are expressed as percentage of disc height index between post- and pre-puncture, as %DHI=(post-punctured DHI/pre-punctured DHI)x100. This value is directly proportional to the degree of disc degeneration [17,19]. We did not observe any statistically significant differences in

%DHI between groups, although values for the group 21-G are lower than for the 25-G, indicating that a higher caliber needle induces a higher degree of disc degeneration (Figure 2b).

Evaluation of ECM and cellular content within the IVD

Histological grading score

For quantification of the degree of degeneration within the disc, we have used a histological grading scale that evaluates 5 categories of IVD degenerative alterations: Cellularity of the AF, Morphology of the AF, Border between the AF and NP, Cellularity of the NP and Morphology of the NP, each classified with a score between 1 (normal disc) and 5 (highly degenerated disc). Such a scale has been presented before [17]. The overall score per group is presented in Figure 2c. As we can see, the 21-G needle presents higher histological degenerative traits than the 25-G needle, with a statistically significant difference observed at 2 weeks (*$p \leq 0.05$). This result shows that a higher caliber needle results in more prominent disc degeneration. We can see as an example the disrupted border between NP and AF and serpentine fibers in the AF, by Safranin O staining, for the 21-G at 2 weeks (Figure 2e), as opposed to the control tissue (Figure 2d).

GAG quantification in the NP

GAG quantification was performed in the fresh tissue, using the Blyscan sulfated proteoglycan assay. Only the NP tissue inside the IVD was analysed and not the extruded tissue within the hernia site. Results are presented in Figure 3. A clear trend can be seen between 2 weeks and 6 weeks for both needle gauges, with a statistically significant difference (*$p \leq 0.05$) obtained only for the 25-G needle. This result seem to indicate that the lesion caused a temporary increase in GAG content that returns to basal levels in the long term. Other studies have shown a decrease in GAG content after needle puncture up to 4 weeks [17], or no alterations up to 4 weeks [21].

Collagen quantification

For quantification of the collagen present in the IVD extracellular matrix, we have performed immunofluorescence against Collagen type II (Col II) and Picrosirius red staining that identifies Collagen type I (Col I) and type III (Col III). For both analyses, a semi-quantitative grading score of

the stained sections was performed. For all groups, we have found higher amounts of Col II in the NP than in the AF (Figure 4a-f) and higher amounts of Col I+III in the AF than in the NP (Figure 4g-l). This reciprocal distribution of Col I and Col II within the disc, with Col I dominating in the AF and Col I dominating in the NP, has been shown before [22,23].

To what regards Col II levels, we have found an overall decrease in the NP and an overall increase in the AF for all groups, with respect to control. Also, there seems to be a decrease in Col II content at 2 weeks post-injury, which is then recovered after 6 weeks. The same trend is found for Col I, which we have quantified only in the AF, given the nature of the Picrosirius red staining, which identifies the birefringence of collagen fiber bundles and poor presence in the NP. This staining allows the identification of large type I collagen fibers, by their yellow/orange/red birefringence, and thin type III collagen fibers, by their green birefringence, under polarized light. Col I and Col III have overlapping distributions [24]. Especially for the large Col I fibers, there is a decrease in its content for all groups, with respect to control. Moreover, it seems that there is a recovery in Col I content at 6 weeks post-injury, with respect to the 2 weeks time point. These results seem to indicate a spontaneous recovery of the injured disc, in terms of extracellular matrix collagen content.

Quantification of cell death

Quantitative assessment of cell death within the lesioned IVD was performed by the TUNEL assay and is shown as percentage of positive cells in annulus fibrosus (AF, Figure 5a) and in nucleus pulposus (NP, Figure 5b). Statistical analysis revealed no differences between groups for AF. Results for the NP demonstrate a significantly higher number of apoptotic cells for the 21-G needle, with respect to the 25-G needle at 2 and 6 weeks (***$p \leq 0.0001$). Moreover, there is an increase in cell death from 2 to 6 weeks for both groups, with statistically significance observed only for the 25-G group (**$p \leq 0.001$). Overall, results indicate the lesion has caused an increase in apoptosis with increasing needle size but, moreover, apoptosis is intensified through time for both needle sizes.

Histopathological evaluation within the hernia

Hernia volume

Apart from the histological alterations induced by needle puncture within the disc confinement, also herniation of the NP to the outer disc space was found for both groups. Hernia volume was systematically analysed by histology, which allows the fine identification of herniated tissue throughout the whole IVD section and is presented here as an alternative to the MRI technique for hernia quantification. Measurements were made by hernia area delimitation on section at precise intervals throughout the IVD (Supplementary material 2). 2 weeks post-lesion, 25-G group presented significantly smaller hernias than 21-G group (Figure 6a-d). At 6 weeks, both groups presented a reduction in hernia volume, with respect to 2 weeks, with hernias almost completely disappearing in the 25-G group. It seems that for both groups the hernias formed after lesion spontaneously regressed. This phenomenon of hernia spontaneous regression has been increasingly reported [25-27] and it is, moreover, in agreement with our results for IVD degeneration, indicating an overall spontaneous reduction in both the degree of IVD degeneration and herniation along time.

We have also quantified the number of hematoxylin-positive cells within the central section of each hernia and determined the mean number per group, values are presented in Figure 6a. Although the number of cells seems to correspond to the hernia volume for each group, there is a slight higher density of cells for both lesions at 2 weeks (25-G: 42.4 cells/mm^2; 21-G: 40.1 cells/mm^2), than at 6 weeks (25-G: 29.2 cells/mm^2; 21-G: 35.5 cells/mm^2).

Quantification of cell death

Quantification of cell death within the herniated tissue was performed by the TUNEL assay and is shown as percentage of positive cells in Figure 5c,f,g. Results show a decrease in cell death between 2 and 6 weeks after lesion, with the 21-G lesion inducing higher proportion of cell death within the hernia than the 25-G lesion, identically to what was observed for the annulus fibrosus and annulus pulposus (Figure 5a,b).

ECM content

The main IVD extracellular components, collagen and proteoglycans, were quantified within the herniated tissue, as percentage area of collagen type I, calculated from Masson's trichrome staining and percentage area of proteoglycans, calculated from Safranin O staining. Results indicate the same levels for 25-G and 21-G groups, for both proteoglycans and collagen type I, with a reduction between 2 and 6 weeks for proteoglycans and no alteration between 2 and 6 weeks for collagen type I (Figure 7a). Collagen type II has also been assessed by immunofluorescence but no positivity was present for any of the hernias in study (Supplementary material 1a).

Matrix metalloproteinases

Assessment of matrix metalloproteinases presence within the hernia was made by quantifying MMP3 and MMP14, which are both responsible for ECM breakdown and shown to be involved in IVD degeneration [28,29]. As we can see, there is higher amount of MMP3 for the 21-G group at 2 weeks, remaining with high expression at 6 weeks, instead the 25-G group presents higher values only at 6 weeks (Figure 7b,c,d). For MMP14 there are no significant differences between groups (Figure 7b,e,f).

Macrophage immunoreactivity

The phenomenon of hernia regression has been associated with the inflammatory response from the host tissue [30], so that we have analysed macrophage immunoreactivity within the hernia site, by immunohistochemistry against CD68 (ED1). Results show an increased positivity 2 weeks after lesion, which diminishes after 6 weeks for both groups. The 21-G needle puncture results in a higher number of macrophages present at the herniation site, with respect to the 25-G needle group (Figure 8a-c). This result parallels the dimension of the hernia formed in each group, as detailed before, probably indicating that a more extended hernia induces a higher number of macrophages needed at the hernia site. This may explain the regression in hernia size that occurs between 2 and 6 weeks post-lesion. We have not detected any CD68 positivity within the IVD for any of the groups analysed.

Discussion

This study investigates mechanisms of traumatic IVD degeneration and herniation, using a rat caudal puncture model. This model has been proposed before [8,17], but never analysed together with herniation features in the same animals.

We have selected the rat caudal puncture model since it involves a significantly less invasive surgical procedure than the lumbar model, which requires abdominal incision and complete exposure of the peritoneal cavity of the animal. This model has been increasingly used in studying disc degeneration and, although it may not fully reproduce the complex features of disc degeneration at higher levels of the spine, it is a very reproducible, low cost, efficient and significantly less invasive technique than alternative methods. Obviously the relevance to humans presents limitations and extrapolation factors must be considered, such as the different mechanical loading, the different disc size, which affects cell nutrition and diffusion, the presence of notochordal cells within the nucleus pulposus and the unequal growth of the epiphyseal plate [5]. Particularly, the different mechanical loading and the different proximity to neural structures in caudal vs lumbar IVDs, are likely to result in important differences in herniation behavior and volume across caudal vs lumbar regions.

We have induced IVD lesion with two caliber needle punctures, 25-G and 21-G and demonstrate that the size of injury was associated with severity of disc degeneration, in the same line to what has been reported before [18,31]. While numerous reports on animal models have described the degeneration features within the IVD [reviewed in 31], this is the first study addressing the degeneration and herniation in the same model. The study of the mechanisms of disc herniation is poorly uncovered in animal studies and reports are mainly confined to diagnostic imaging techniques, although this is indeed one of the main clinically relevant features of IVD pathophysiology.

We have found here that the occurrence of hernia is proportional to the lesion created and that it

spontaneously regresses along time. The phenomenon of hernia regression has been long observed clinically by magnetic resonance imaging and the few studies that have addressed the histological mechanisms behind it, have associated hernia regression with the inflammatory response from the host tissue [25,30,32]. For this reason we have quantified CD68+ macrophages and observed that they concentrate within the herniated tissue site and its presence is proportional to the hernia volume. This may probably indicate that a more extended hernia induces a higher number of infiltrating macrophages needed at the hernia site and this may contribute to explain the regression in hernia size that occurs between 2 and 6 weeks post-lesion. Worth noticing, we have not detected any positivity for CD68 within the IVD itself (Supplementary material 1b-d), so for this reason we believe that the macrophages have migrated from surrounding tissues or differentiated from monocytes *in loco* rather than being resident cells. In fact, analysis of human lumbar herniated tissue, indicates that macrophages derived from monocytes migrating to the hernia are key factors involved in hernia regression, capable of active phagocytosis of the herniated tissue, through lysosomes filled with collagen-degrading enzymes [30,32]. Macrophages also directly secrete lysosomal enzymes (exocytosis) that break down intercellular substances [33,34].

We have also observed that apoptosis, as well as MMP3, is increased in the hernia following a high caliber lesion, indicating that not only macrophage action may be responsible for hernia resorption, although it is difficult to unravel which mechanism is a cause or a consequence of hernia regression. To what regards MMP3, higher degradative enzyme concentrations and elevated enzyme activity have been shown in degenerating discs compared with normal discs [29,35]. Matrix metalloproteinases are indeed believed to be the major proteolytic enzymes responsible for ECM degradation in the IVD, thereby contributing to pathological tissue destruction and allowing normal remodeling [reviewed in 28].

Finally, there are some limitations to this study that deserve consideration. A clinically relevant model should mimic the human IVD pathology, which in most of the cases is directly associated with pain. Still, in our study we proposed to understand cell and tissue mechanisms behind disc

degeneration and herniation, so that we did not access pain behaviour here. The association between disc degeneration, herniation and pain may be more clinically relevant, so that the development of models such as the one by Kim et al. may need to be developed for the caudal lesion in the future [13]. Finally, given the reduced number of animais analysed, we must interpret the results presented here with caution. Still, few studies have analysed herniation and hernia resoption in detail in animal models, so that hopefully we may contribute to unravel such complex mechanisms.

Conclusions

This study explored an *in vivo* rat model of IVD caudal needle puncture as a non-invasive, cost-effective, efficient and reproducible method for the analysis of the pathophysiological features of IVD degeneration and herniation. We have characterized along time the histological, radiographical and biochemical features behind disc degeneration in the rat caudal IVD, caused by two different types of lesion. Moreover, we have analysed IVD herniation coupled to IVD degeneration in the same rat model. The preliminary results obtained may be important to unravel the complex mechanisms behind IVD degeneration and to design new tissue engineering approaches for IVD regeneration.

Acknowledgments

The authors acknowledge the Bioengineered Microenvironments for Repair/Regeneration Team at INEB for helpful suggestions, António Ribeiro for technical assistance with histological procedures, Célia Lopes and Prof. Eduardo Rocha for providing the anti-CD68 antibody, Alexandra Rêma and Prof. Fátima Gartner for performing the CD68 immunostaining, Prof. Pedro Oliveira for statistical advice and Prof. Kharen Doyle for English revision. Financial support was provided by North Region Operational Program (ON.2), in the framework of the Project on Biomedical Engineering for Regenerative Therapies and Cancer - NORTE- 07-0124-FEDER-000005, through Quadro de Referência Estratégico Nacional (QREN), and also by FCT – Fundação para a Ciência e a

Tecnologia through Fellowship SFRH/BDP/87071/2012 to Carla Cunha. The authors declare no potential conflict of interests.

References

1. Andersson GB (1999) Epidemiological features of chronic low-back pain. Lancet 354: 581-585.

2. Silva-Correia J, Correia SI, Oliveira JM, Reis RL (2013) Tissue engineering strategies applied in the regeneration of the human intervertebral disk. Biotechnol Adv 31: 1514-1531.

3. Anderson DG, Tannoury C (2005) Molecular pathogenic factors in symptomatic disc degeneration. Spine J 5: 260S-266S.

4. Sivan SS, Hayes AJ, Wachtel E, Caterson B, Merkher Y, et al. (2014) Biochemical composition and turnover of the extracellular matrix of the normal and degenerate intervertebral disc. Eur Spine J 23 Suppl 3: S344-353.

5. Alini M, Eisenstein SM, Ito K, Little C, Kettler AA, et al. (2008) Are animal models useful for studying human disc disorders/degeneration? Eur Spine J 17: 2-19.

6. Kim J, Yang SJ, Kim H, Kim Y, Park JB, et al. (2012) Effect of Shear Force on Intervertebral Disc (IVD) Degeneration: An In Vivo Rat Study. Ann Biomed Eng 40: 1996-2004.

7. Wang YJ, Shi Q, Lu WW, Cheung KCM, Darowish M, et al. (2006) Cervical intervertebral disc degeneration induced by unbalanced dynamic and static forces: A novel in vivo rat model. Spine 31: 1532-1538.

8. Zhang HN, La Marca F, Hollister SJ, Goldstein SA, Lin CY (2009) Developing consistently reproducible intervertebral disc degeneration at rat caudal spine by using needle puncture Laboratory investigation. Journal of Neurosurgery-Spine 10: 522-530.

9. Boxberger JI, Auerbach JD, Sen S, Elliott DM (2008) An in vivo model of reduced nucleus pulposus glycosaminoglycan content in the rat lumbar intervertebral disc. Spine 33: 146-154.

10. Norcross JP, Lester GE, Weinhold P, Dahners LE (2003) An in vivo model of degenerative disc disease. Journal of Orthopaedic Research 21: 183-188.

11. Murrell W, Sanford E, Anderberg L, Cavanagh B, Mackay-Sim A (2009) Olfactory stem cells can be induced to express chondrogenic phenotype in a rat intervertebral disc injury model. Spine Journal 9: 585-594.

12. Rousseau MA, Bass EC, Lotz JC (2004) Ventral approach to the lumbar spine of the Sprague-Dawley rat. Lab Animal 33: 43-45.

13. Kim JS, Kroin JS, Li X, An HS, Buvanendran A, et al. (2011) The rat intervertebral disk degeneration pain model: relationships between biological and structural alterations and pain. Arthritis Res Ther 13: R165.

14. Inoue G, Ohtori S, Aoki Y, Ozawa T, Doya H, et al. (2006) Exposure of the nucleus pulposus to the outside of the anulus fibrosus induces nerve injury and regeneration of the afferent fibers innervating the lumbar intervertebral discs in rats. Spine (Phila Pa 1976) 31: 1433-1438.

15. Li YJ, Xi CY, Niu M, Chi ZY, Liu XQ, et al. (2011) Activation of satellite cells in the dorsal root ganglia in a disc-punctured rat model. Journal of Orthopaedic Science 16: 433-438.

16. Crevensten G, Walsh AJL, Ananthakrishnan D, Page P, Wahba GM, et al. (2004) Intervertebral disc cell therapy for regeneration: Mesenchymal stem cell implantation in rat intervertebral discs. Annals of Biomedical Engineering 32: 430-434.

17. Han B, Zhu K, Li FC, Xiao YX, Feng J, et al. (2008) A simple disc degeneration model induced by percutaneous needle puncture in the rat tail. Spine 33: 1925-1934.

18. Keorochana G, Johnson JS, Taghavi CE, Liao JC, Lee KB, et al. (2010) The effect of needle size inducing degeneration in the rat caudal disc: evaluation using radiograph, magnetic resonance imaging, histology, and immunohistochemistry. Spine Journal 10: 1014-1023.

19. Masuda K, Aota Y, Muehleman C, Imai Y, Okuma M, et al. (2005) A novel rabbit model of mild, reproducible disc degeneration by an anulus needle puncture: Correlation between the degree of disc injury and radiological and histological appearances of disc degeneration. Spine 30: 5-14.

20. Ruifrok AC, Johnston DA (2001) Quantification of histochemical staining by color deconvolution. Anal Quant Cytol Histol 23: 291-299.

21. Hsieh AH, Hwang D, Ryan DA, Freeman AK, Kim H (2009) Degenerative anular changes induced by puncture are associated with insufficiency of disc biomechanical function. Spine (Phila Pa 1976) 34: 998-1005.

22. Eyre DR, Muir H (1976) Types I and II collagens in intervertebral disc. Interchanging radial distributions in annulus fibrosus. Biochem J 157: 267-270.

23. Eyre DR, Muir H (1977) Quantitative analysis of types I and II collagens in human intervertebral discs at various ages. Biochim Biophys Acta 492: 29-42.

24. Roberts S, Menage J, Duance V, Wotton S, Ayad S (1991) 1991 Volvo Award in basic sciences. Collagen types around the cells of the intervertebral disc and cartilage end plate: an immunolocalization study. Spine (Phila Pa 1976) 16: 1030-1038.

25. Autio RA, Karppinen J, Niinimaki J, Ojala R, Kurunlahti M, et al. (2006) Determinants of spontaneous resorption of intervertebral disc herniations. Spine (Phila Pa 1976) 31: 1247-1252.

26. Martinez-Quinones JV, Aso-Escario J, Consolini F, Arregui-Calvo R (2010) Spontaneous regression from intervertebral disc herniation. Propos of a series of 37 cases. Neurocirugia (Astur) 21: 108-117.

27. Slavin KV, Raja A, Thornton J, Wagner FC, Jr. (2001) Spontaneous regression of a large lumbar disc herniation: report of an illustrative case. Surg Neurol 56: 333-336; discussion 337.

28. Vo NV, Hartman RA, Yurube T, Jacobs LJ, Sowa GA, et al. (2013) Expression and regulation of metalloproteinases and their inhibitors in intervertebral disc aging and degeneration. Spine J 13: 331-341.

29. Yurube T, Takada T, Suzuki T, Kakutani K, Maeno K, et al. (2012) Rat tail static compression model mimics extracellular matrix metabolic imbalances of matrix metalloproteinases, aggrecanases, and tissue inhibitors of metalloproteinases in intervertebral disc degeneration. Arthritis Res Ther 14: R51.

30. Kawaguchi S, Yamashita T, Yokogushi K, Murakami T, Ohwada O, et al. (2001) Immunophenotypic analysis of the inflammatory infiltrates in herniated intervertebral discs. Spine (Phila Pa 1976) 26: 1209-1214.

31. Elliott DM, Yerramalli CS, Beckstein JC, Boxberger JI, Johannessen W, et al. (2008) The effect of relative needle diameter in puncture and sham injection animal models of degeneration. Spine (Phila Pa 1976) 33: 588-596.

32. Kobayashi S, Meir A, Kokubo Y, Uchida K, Takeno K, et al. (2009) Ultrastructural analysis on lumbar disc herniation using surgical specimens: role of neovascularization and macrophages in hernias. Spine (Phila Pa 1976) 34: 655-662.

33. Henson PM (1980) Mechanisms of exocytosis in phagocytic inflammatory cells. Parke-Davis Award Lecture. Am J Pathol 101: 494-511.

34. Unanue ER (1976) Secretory function of mononuclear phagocytes: a review. Am J Pathol 83: 396-418.

35. Roberts S, Caterson B, Menage J, Evans EH, Jaffray DC, et al. (2000) Matrix metalloproteinases and aggrecanase: their role in disorders of the human intervertebral disc. Spine (Phila Pa 1976) 25: 3005-3013.

Figure Legends

Figure 1. Identification of the target discs and puncture. a) Co1/2 is found by palpation and X-ray imaging. Needle puncture into the rat coccygeal intervertebral disc Co6/7, as imaged by X-ray radiography, using a 25-G needle gauge (b) and a 21-G needle gauge (c). d) Home-made 21-G needle cap device leaving 5 mm needle tip exposed. Scale bars: 5 mm.

Figure 2. Percentage of disc height index (%DHI) and Histological grading score. DHI is calculated by DHI=2x(D+E+F)/(A+B+C+G+H+I) from digital radiographs, (b) %DHI=post-punctured DHI/pre-punctured DHIx100, results are shown for 25-G and 21-G needle gauge groups, 2 and 6 weeks after lesion (a). c) Histological grading score, as defined by Han et al., 2008, *p≤0.05. Histological section showing the border between the AF and the NP (arrows), stained by Safranin O/Fast Green, for d) Unlesioned healthy disc and e) 2 weeks post-injury using the 21-G needle, showing disrupted border between NP and AF and serpentine fibers in the AF.

Figure 3. Quantification of sulfated glycosaminoglycans (GAG) present in the nucleus pulposus. The Blyscan assay has been used for 25-G and 21-G needles, 2 and 6 weeks after lesion and values obtained normalized with tissue wet weight. A statistically significant difference was obtained for the 25-G needle between 2 and 6 weeks. *p≤0.05.

Figure 4. Collagen semi-quantitative analysis by collagen type II immunofluorescence and Picrosirius red staining for collagen type I and type III. a) Collagen type II staining score for the AF and the NP, where +=weak, ++=moderate and +++=strong. b-f) Collagen II immunofluorescence (green) is shown for each group, nuclear staining by DAPI is shown in blue. The dashed line sets the border between AF and NP. g) Picrosirius red staining score for collagen type I (large orange/red fibers) and collagen type III (thin green fibers) in the AF only, where +=weak, ++=moderate and +++=strong. h-l) Picrosirius red-stained histological sections for each group showing the larger fibers in orange/red and the thinner fibers in green, under polarized light. Scale bars: 200 µm.

Figure 5. Cell death in the IVD and hernia, as quantified by the TUNEL assay. Percentage of apoptotic cells in the annulus fibrosus (a), in the nucleus pulposus (b) and within the hernia site (c) for 25-G and 21-G needles, 2 and 6 weeks after lesion, presented as MEAN±SD. No difference between groups was observed in the AF; the NP shows increased cell death with increase in needle gauge for both time points. Within the hernia, there is a decrease in cell death between 2 and 6 weeks for both lesions. TUNEL staining at 2 weeks, showing apoptotic cells (green) and nuclear staining DAPI (blue) within the NP for 25-G (d) and 21-G (e) lesions and for the hernia for 25-G (f) and 21-G (g) lesions. **p≤0.001, ***p≤0.0001.

Figure 6. Herniation in the lesioned discs. Hernia volume in mm^3 was quantified for all groups (a). Representative Safranin O staining (red, proteoglycans) is shown, with dashed line outlining the hernia in the section. b) Unlesioned control, c) 25-G needle, 2 weeks, d) 21-G needle, 2 weeks, e) 25-G needle, 6 weeks, f) 21-G needle, 6 weeks. The number on top of the bars corresponds to the mean number of hematoxylin-positive cells counted on the central section of the hernia. Scale bars: 500 µm.

Figure 7. Quantification of ECM components (proteoglycans, collagen type I and matrix metalloproteinases). a) The percentage area within the hernia occupied by proteoglycans (calculated from Safranin O staining) and collagen type I (calculated from Masson's trichrome staining). b) MMP3 and MMP14 immunohistochemistry, showing in brown positive staining, with hematoxylin counterstaining, 2 weeks after lesion for groups 25-G: c) MMP3, e) MMP14 and 21-G: d) MMP3, f) MMP14. Scale bars: 50 µm.

Figure 8. Quantification of macrophages within the hernia. Macrophage identification by CD68 immunohistochemistry is shown in brown, with hematoxylin counterstaining, 2 weeks after lesion for groups 25-G (a) and 21-G (b); the respective quantification of positive cells within the hernia site is presented (c). Scale bars: 200 µm.

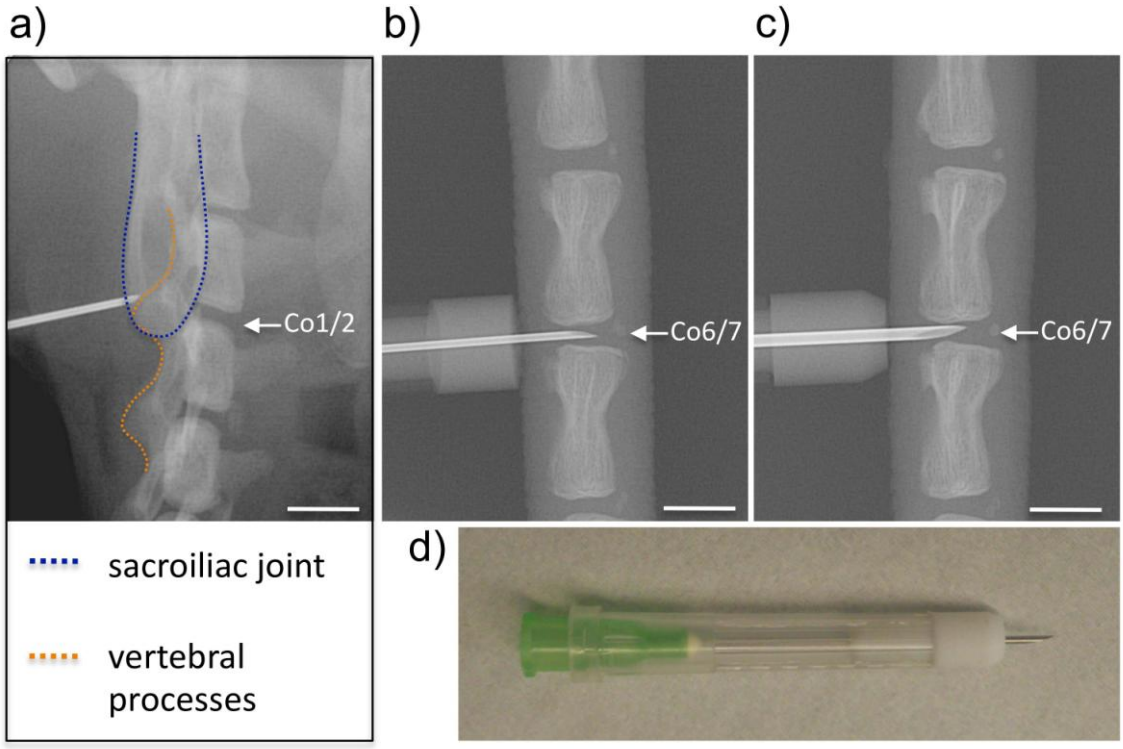

Figure 1

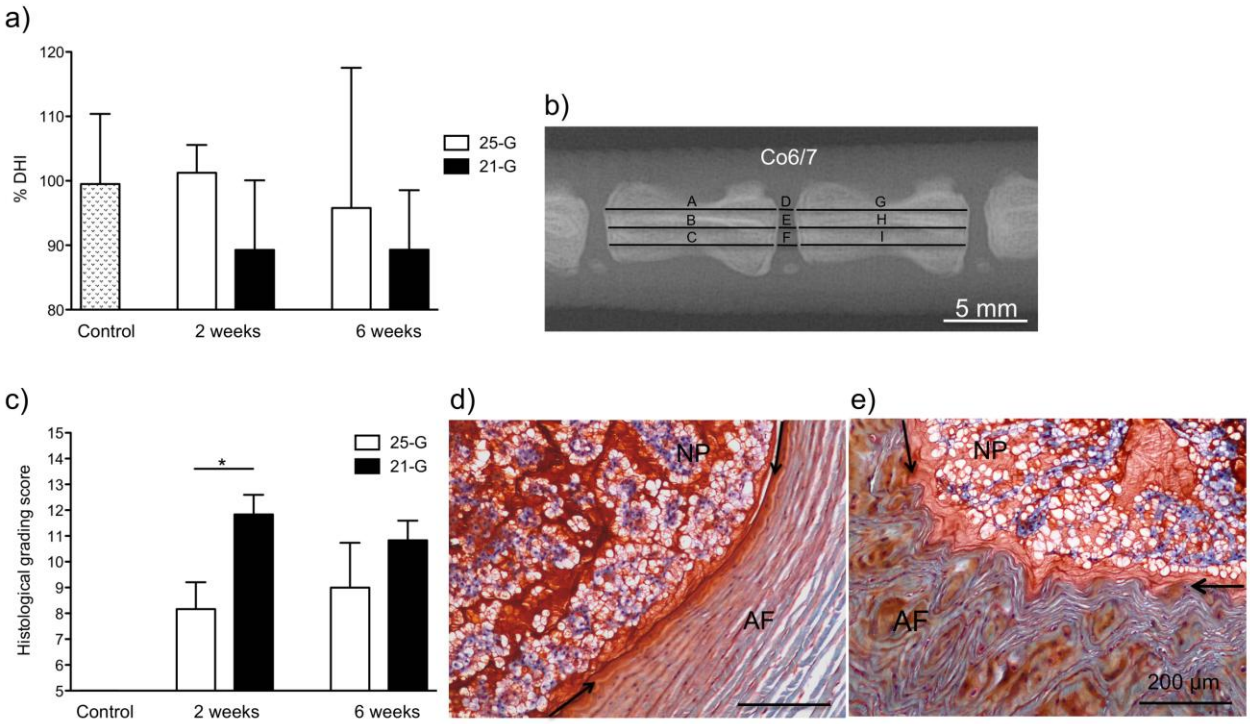

Figure 2

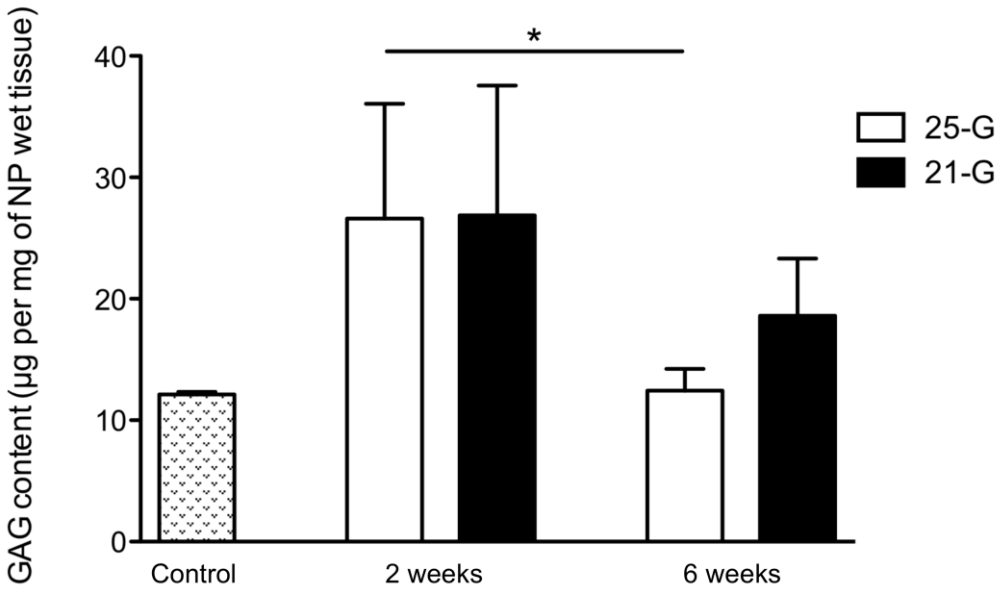

Figure 3

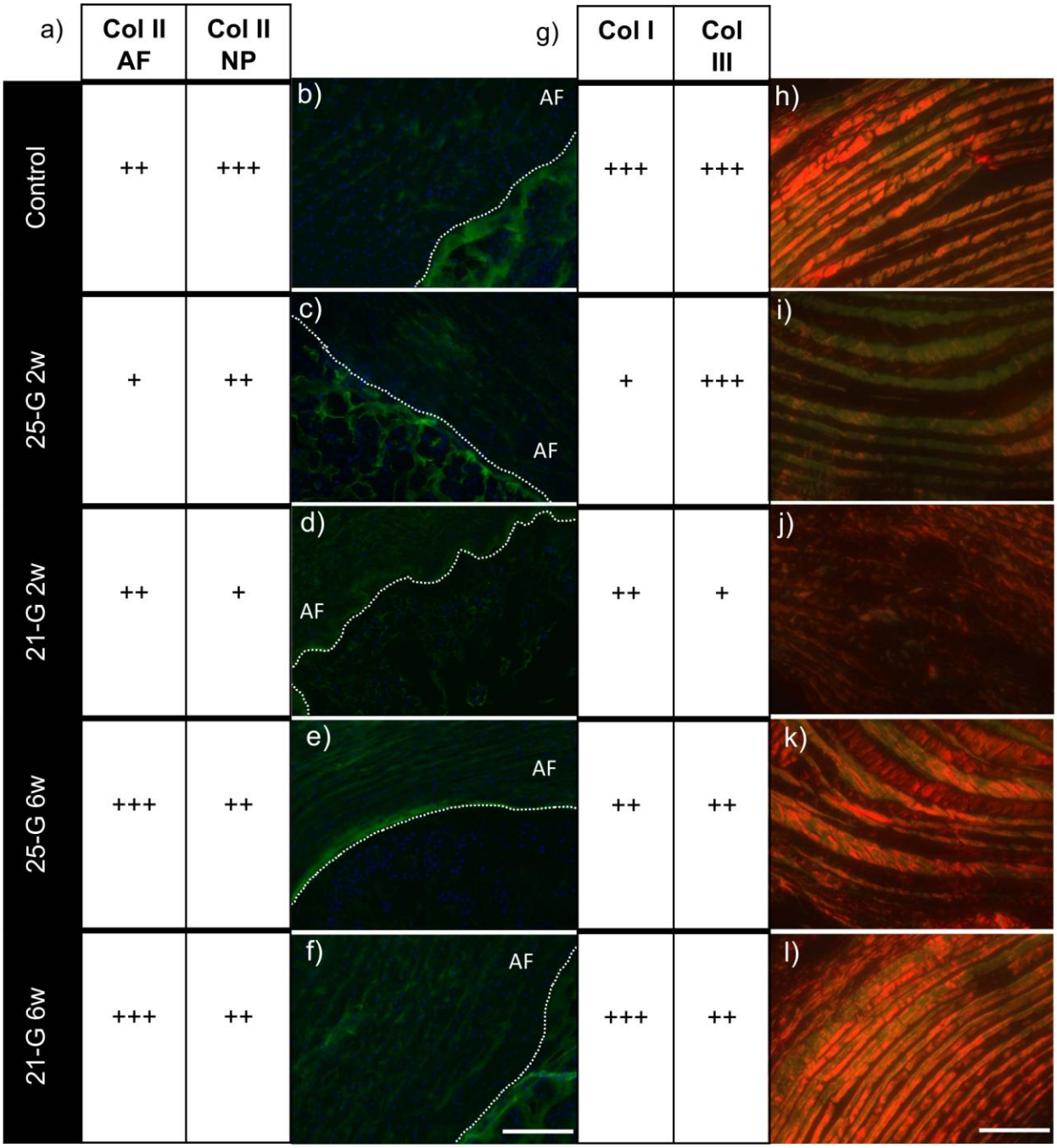

Figure 4

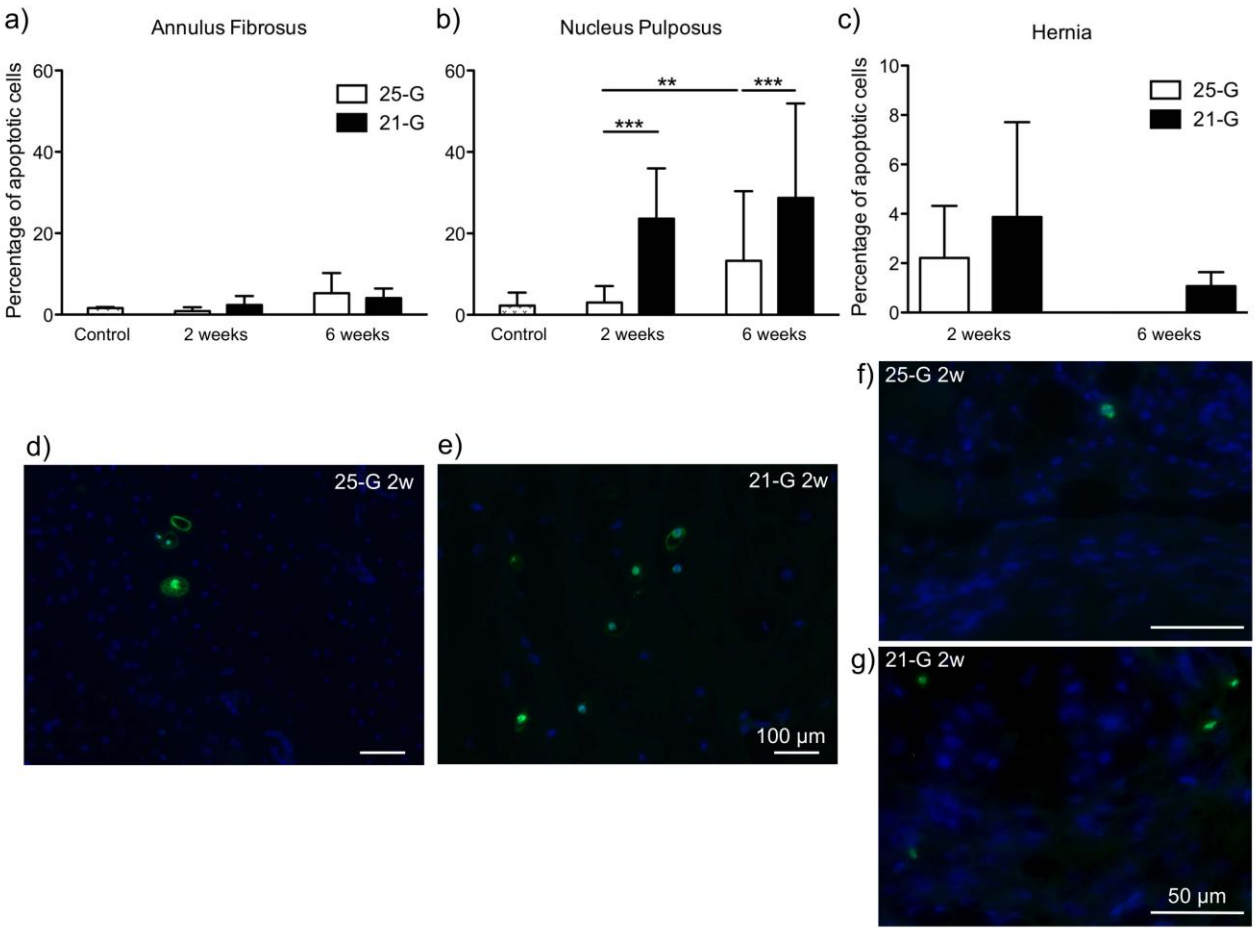

Figure 5

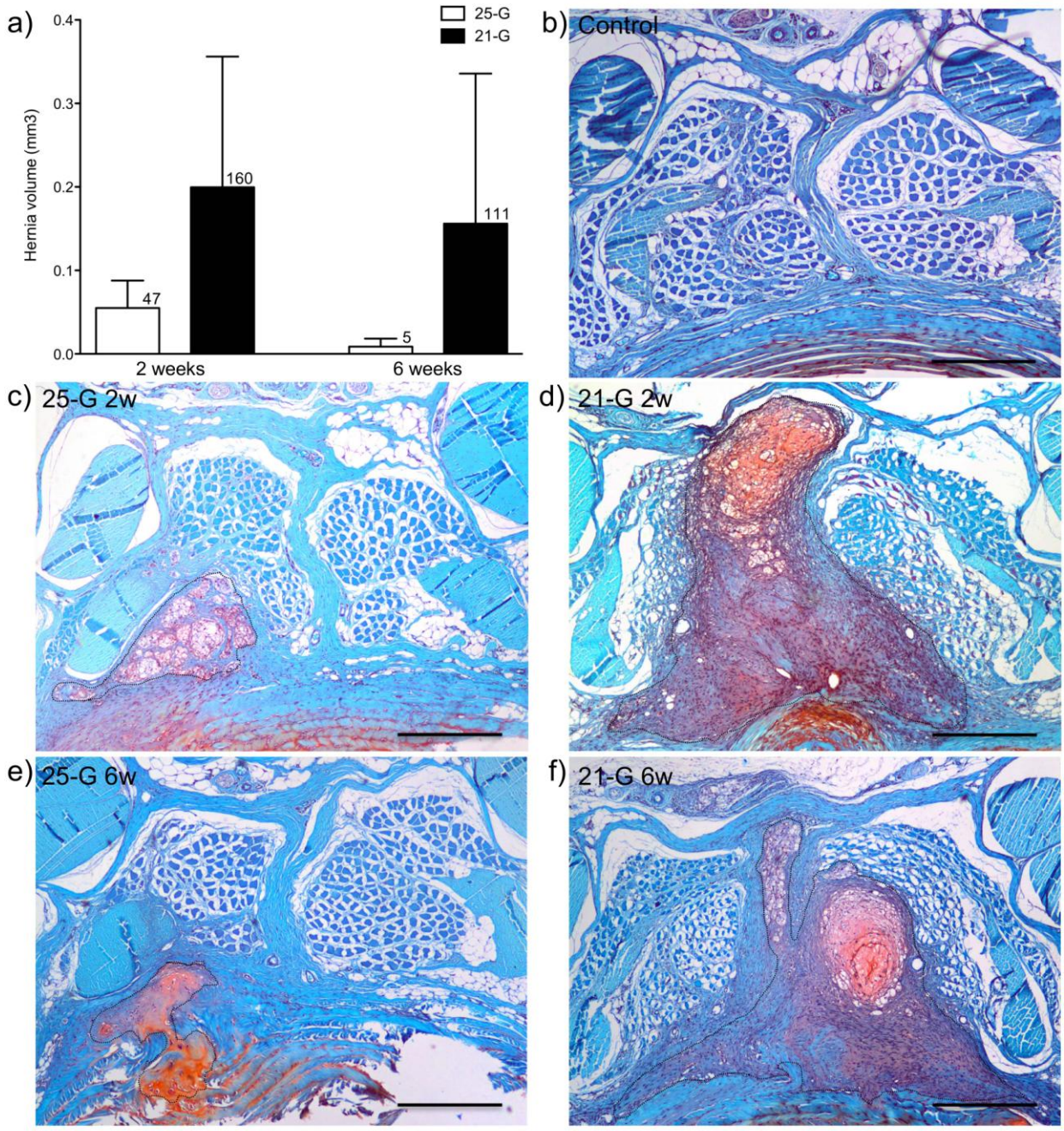

Figure 6

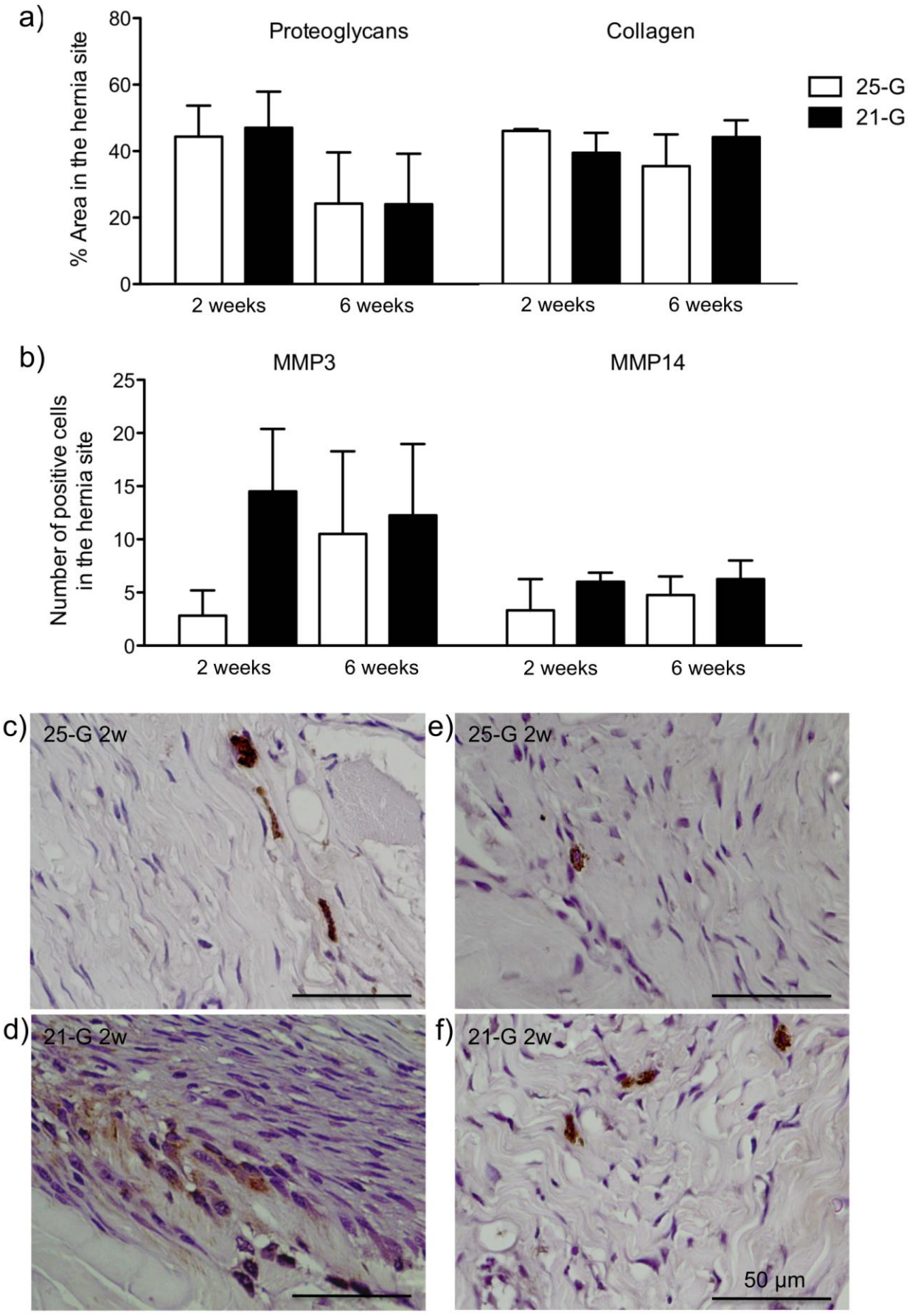

Figure 7

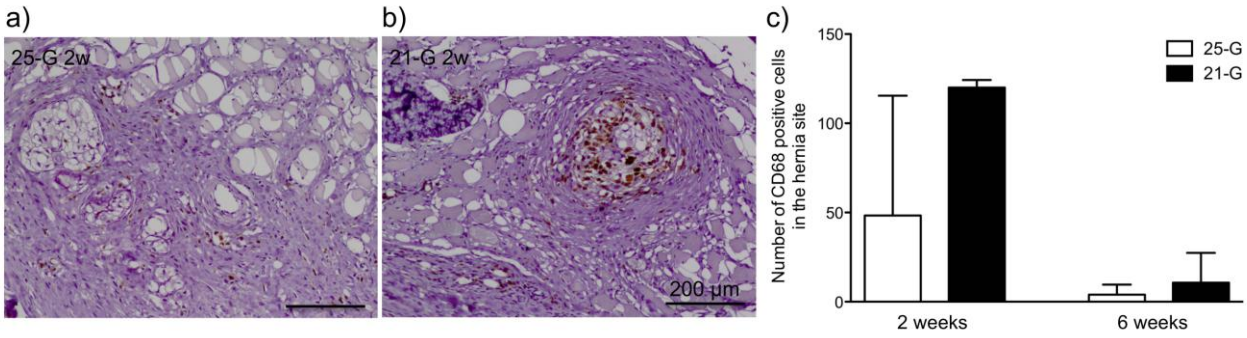

Figure 8